Supporting Information (SI):

Fe_2P-encapsulated in carbon nanowalls decorated by well-dispersed Fe_3C nanodots for efficient hydrogen evolution and oxygen reduction reaction

Liangliang Feng [a], Xiao Zhang [a], Jianfeng Huang [a,*], Danyang He [a], Xiaoyi Li [a], Qianqian Liu [a], Yongqiang Feng [a], Guodong Li [b], Guanghui Xu [c], Liyun Cao [a,*]

[a] *School of Material Science and Engineering, International S&T Cooperation Foundation of Shaanxi Province, Xi'an Key Laboratory of Green Manufacture of Ceramic Materials, Key Laboratory of Auxiliary and Technology for Chemical Industry, Ministry of Education, Shaanxi University of Science and Technology, Xi'an, 710021, China*

[b] *State Key Laboratory of Inorganic Synthesis and Preparative Chemistry, College of Chemistry, Jilin University, Changchun 130012, China*

[c] *Nano Science and Technology Institute, University of Science and Technology of China, Suzhou, 215123, China*

E-mail: huangjf@sust.edu.cn; 2644245930@qq.com

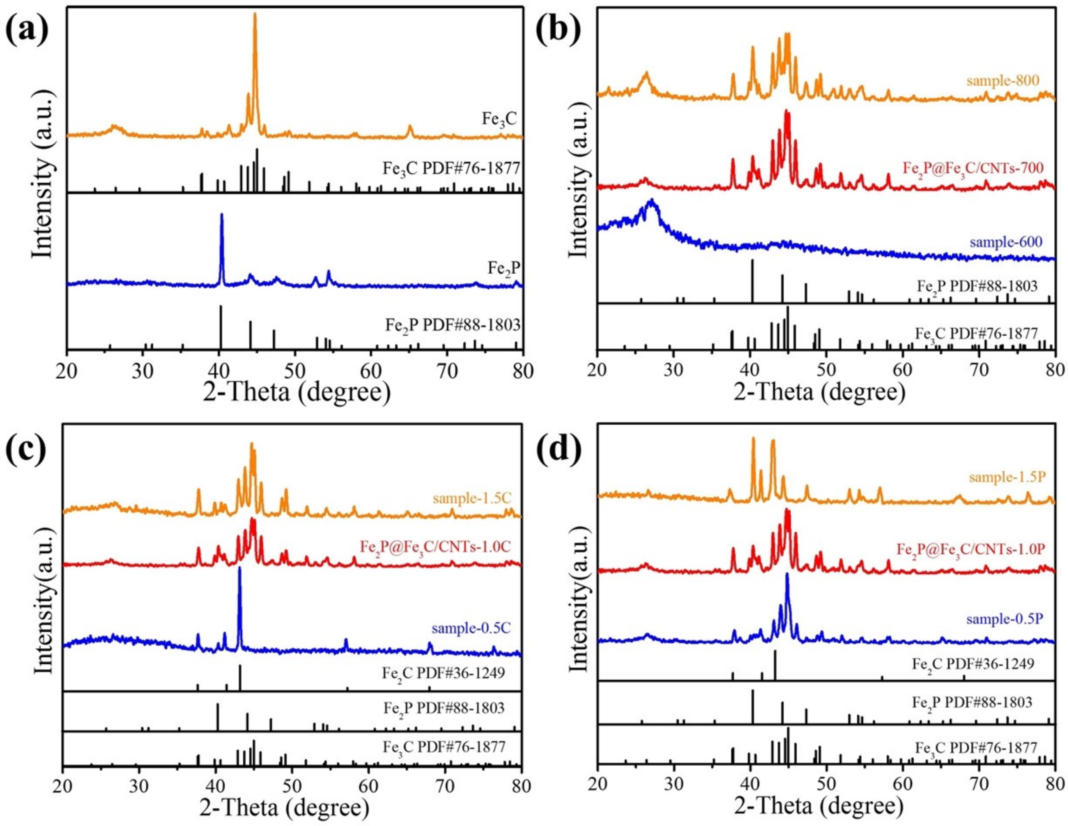

Figure S1. XRD patterns of (a) Fe_3C and Fe_2P; (b) sample-600, Fe_2P@Fe_3C/CNTs-700 and sample-800; (c) sample-0.5C, Fe_2P@Fe_3C/CNTs-1.0C and sample-1.5C; (d) sample-0.5P, Fe_2P@Fe_3C/CNTs-1.0P and sample-1.5P.

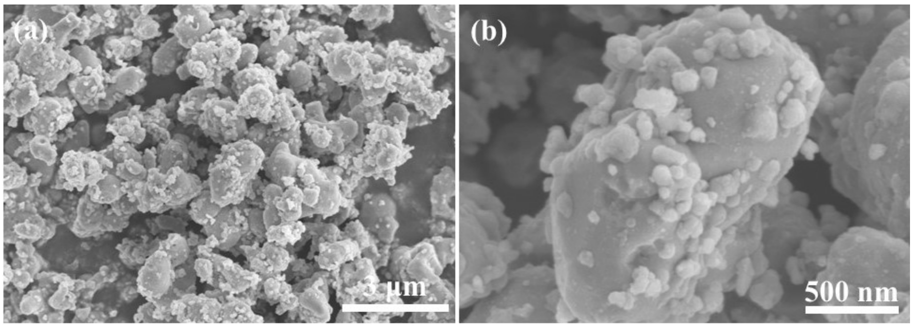

Figure S2. SEM images of sample-0.5C.

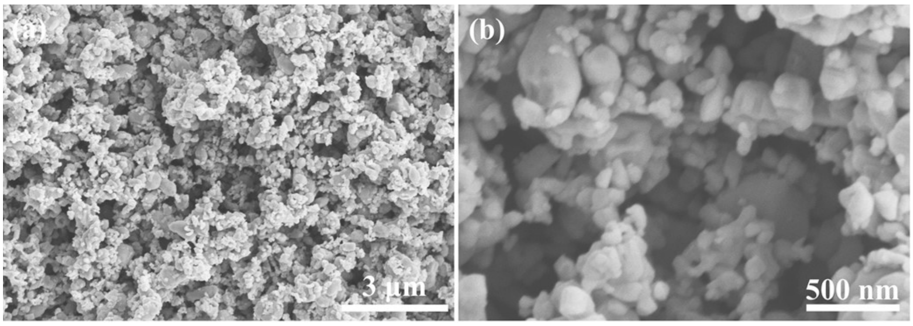

Figure S3. SEM images of sample-1.5P.

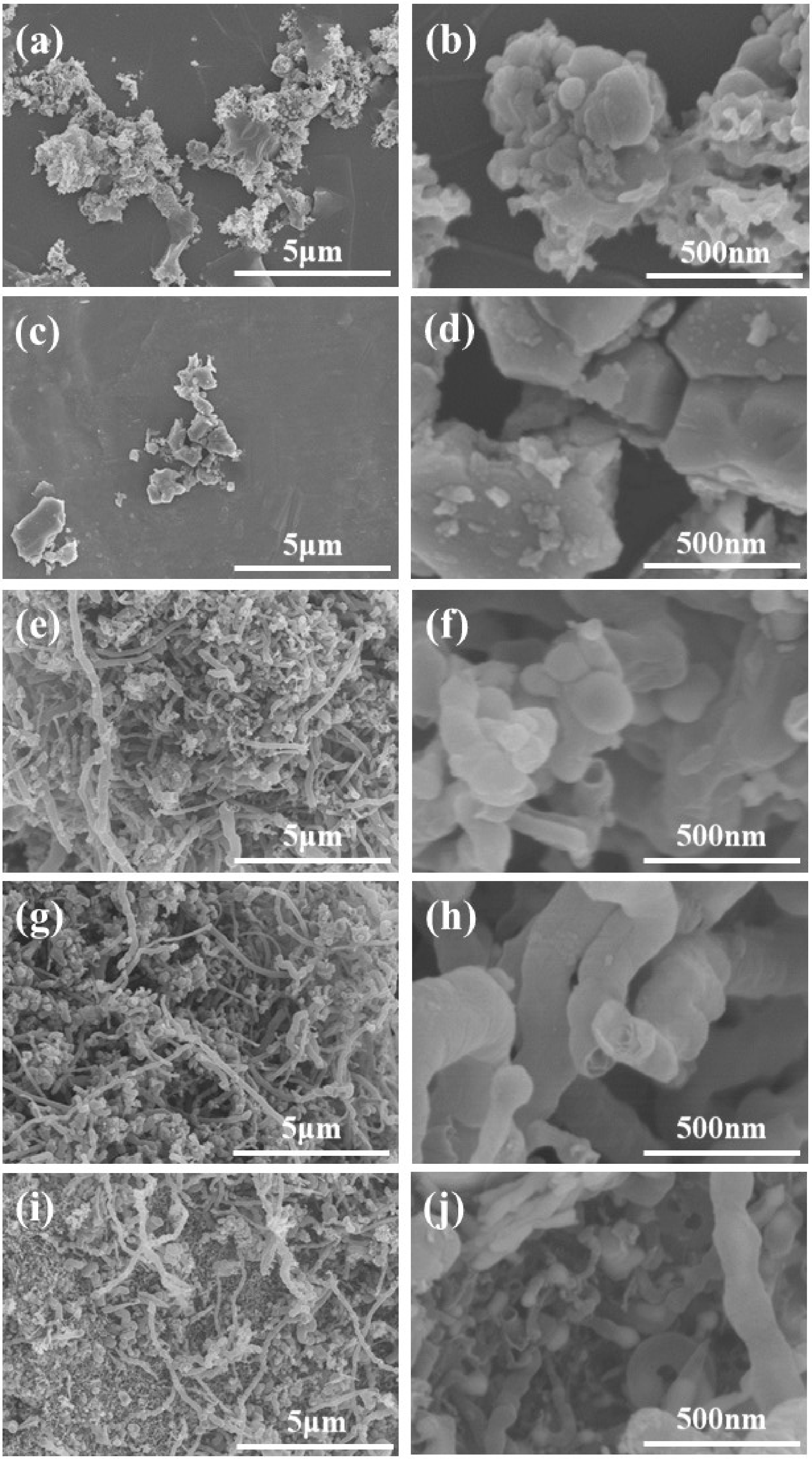

Figure S4. SEM images of (a, b) Fe_3C, (c, d) Fe_2P, (e, f) sampe-800, (g, h) sample-1.5C and (i, j) sample-0.5P.

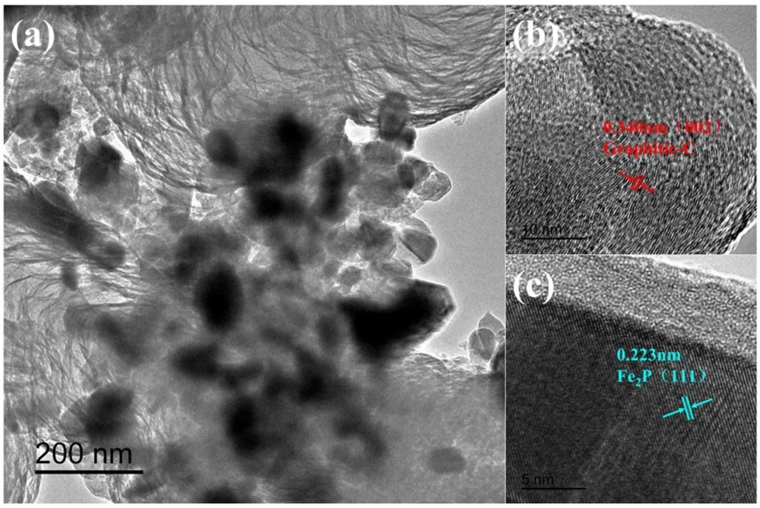

Figure S5. (a) TEM image of $Fe_2P@Fe_3C$/CNTs; (b, c) High-resolution TEM images of $Fe_2P@Fe_3C$/CNTs.

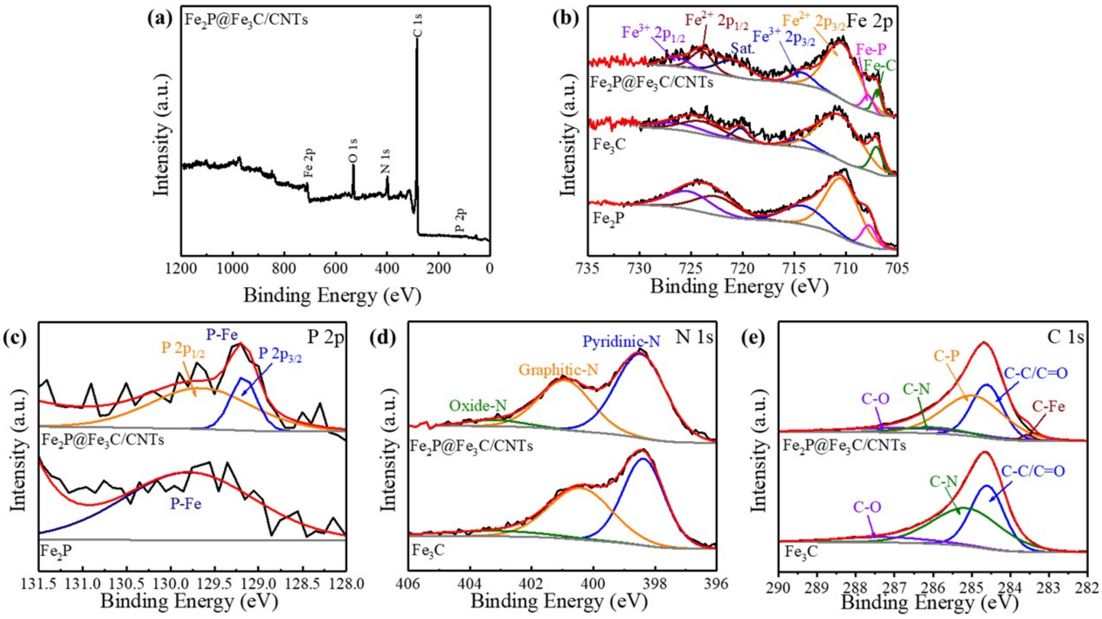

Figure S6. (a) The survey spectrum of $Fe_2P@Fe_3C/CNTs$. High-resolution XPS spectra: (b) Fe 2p, (c) P 2p, (d) N 1s and (e) C1s of $Fe_2P@Fe_3C/CNTs$, Fe_3C and Fe_2P.

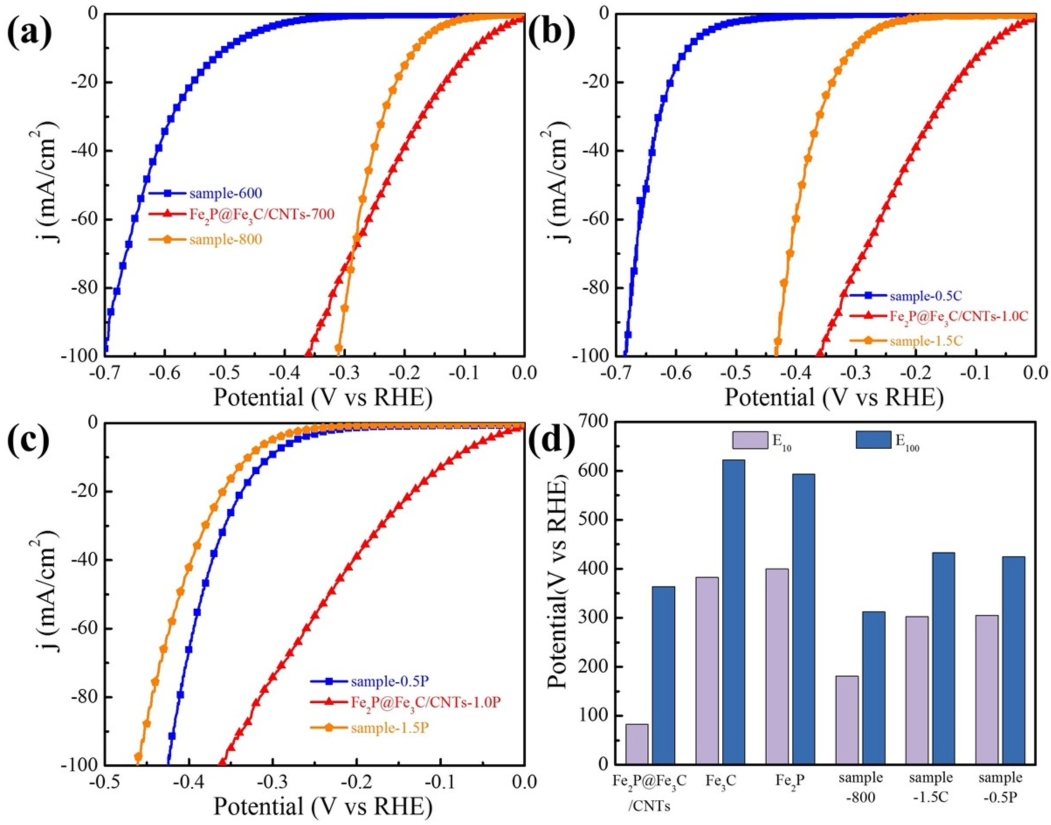

Figure S7. (a) HER Polarization curves of sample-600, $Fe_2P@Fe_3C$/CNTs-700 and sample-800. (b) HER Polarization curves of sample-0.5C, $Fe_2P@Fe_3C$/CNTs-1.0C and sample-1.5C. (c) HER Polarization curves of sample-0.5P, $Fe_2P@Fe_3C$/CNTs-1.0P and sample-1.5P. (d) The potentials of $Fe_2P@Fe_3C$/CNTs, Fe_3C, Fe_2P, sample-800, sample-1.5C and sample-0.5P at 10 mA/cm^2 (E_{10}) and 100 mA/cm^2 (E_{100}).

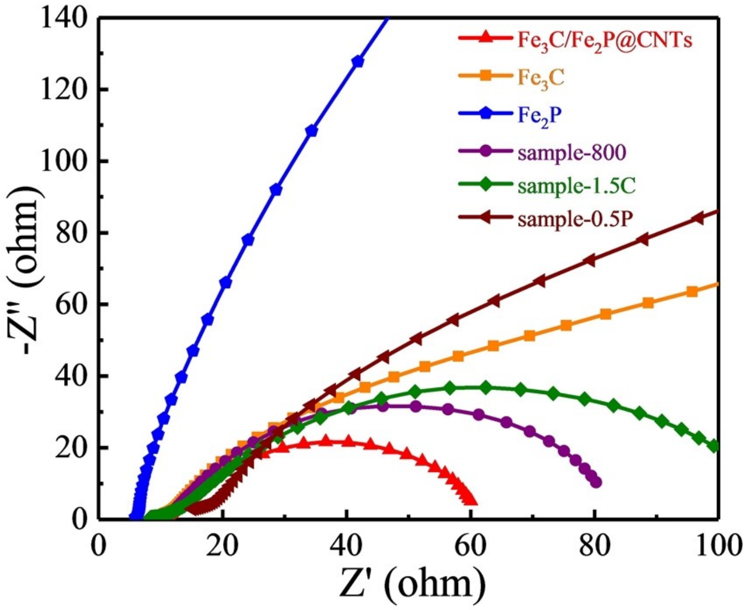

Figure S8. Electrochemical impedance spectroscopy (EIS) Nyquist plots of Fe_2P@Fe_3C/CNTs, Fe_3C, Fe_2P, sample-800, sample-1.5C and sample-0.5P.

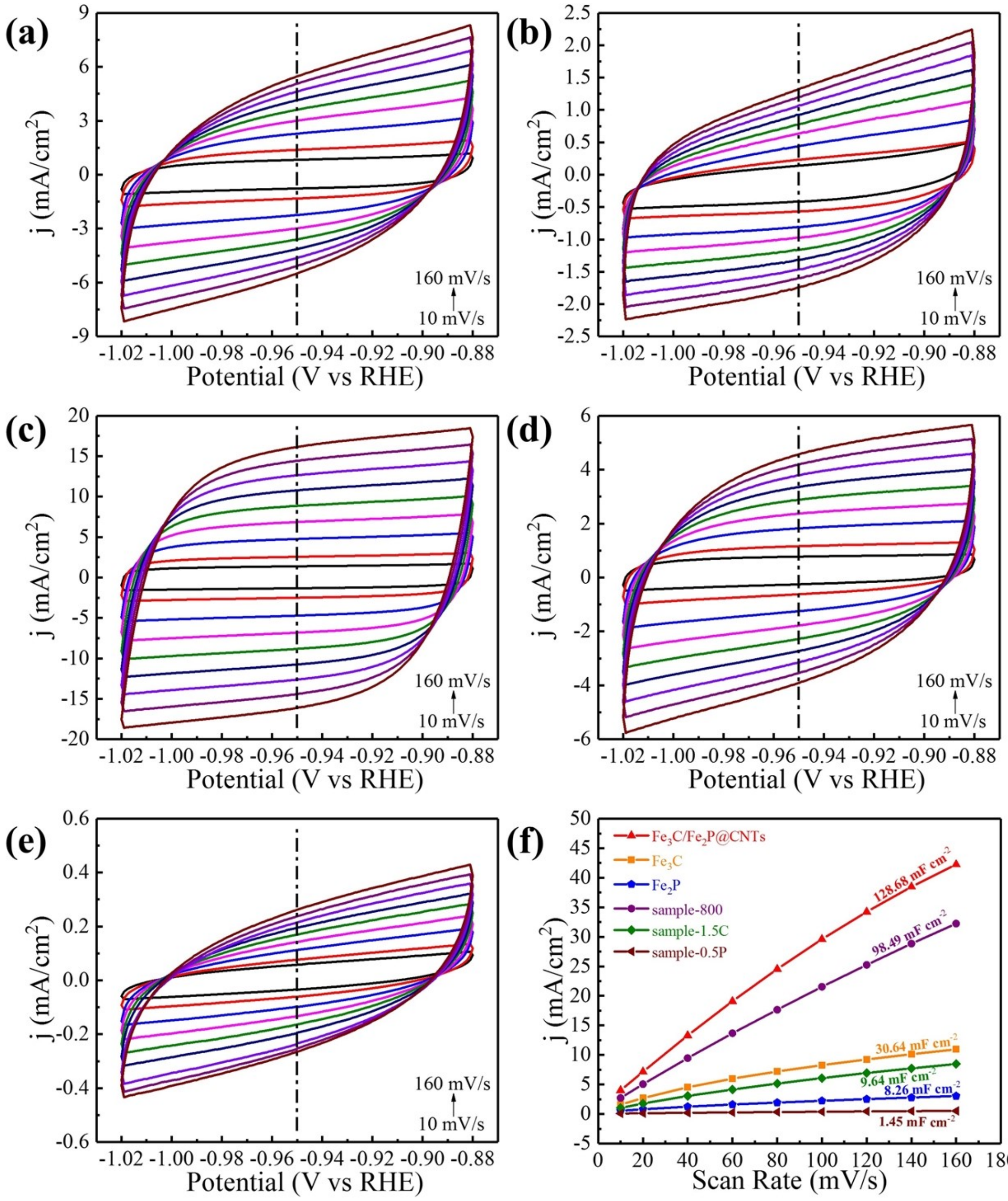

Figure S9. CV curves of (a) Fe_3C, (b) Fe_2P, (c) sample-800, (d) sample-1.5C and (e) sample-0.5P. (f) Electrochemical double-layer capacitance (C_{dl}) of Fe_2P@Fe_3C/CNTs, Fe_3C, Fe_2P, sample-800, sample-1.5C and sample-0.5P.

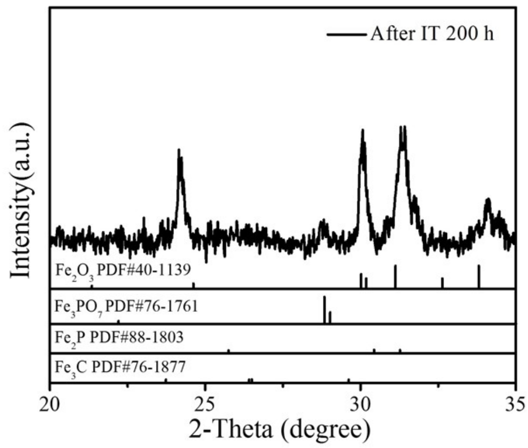

Figure S10. The enlarged XRD pattern of Fe_2P@Fe_3C/CNTs.

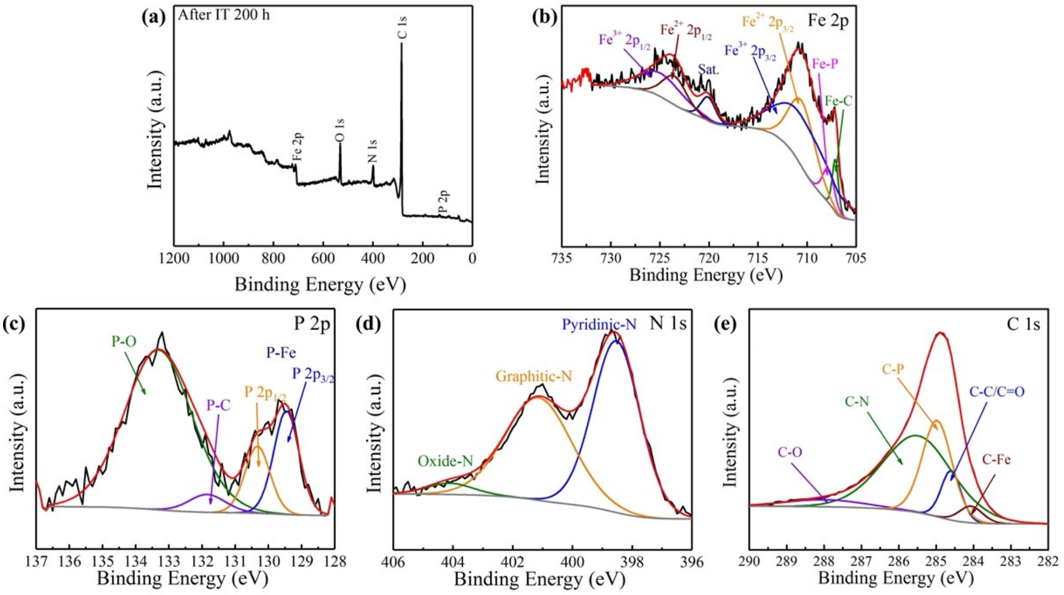

Figure S11. High-resolution XPS spectra: (a) Survey, (b) Fe 2p, (c) P 2p, (d) N 1s and (e) C 1s of $Fe_2P@Fe_3C$/CNTs after the stability test of i-t curve for 200 h at pH 14.

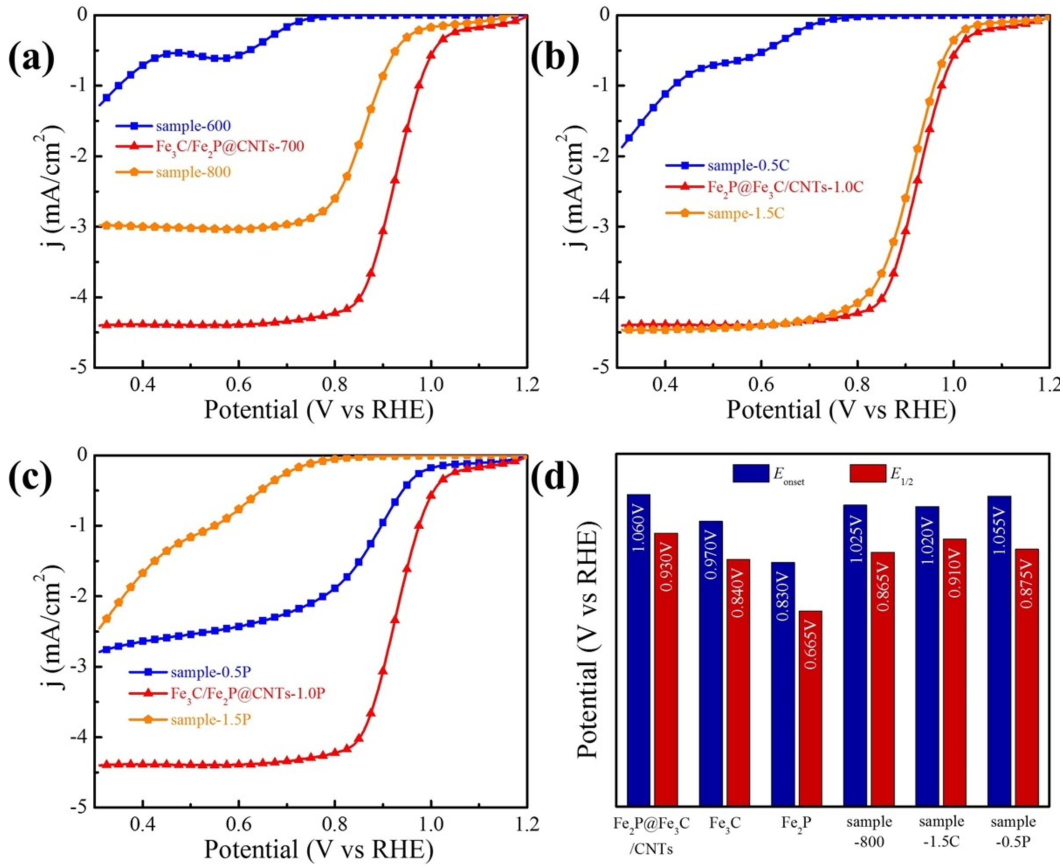

Figure S12. (a) ORR LSV curves of sample-600, Fe_2P@Fe_3C/CNTs-700 and sample-800; (b) ORR LSV curves of sample-0.5C, Fe_2P@Fe_3C/CNTs-1.0C and sample-1.5C; (c) ORR LSV curves of sample-0.5P, Fe_2P@Fe_3C/CNTs-1.0P and sample-1.5P; (d) Onset potential (E_{oneset}) and half-wave potential ($E_{1/2}$) of Fe_2P@Fe_3C/CNTs, Fe_3C, Fe_2P, sample-800, sample-1.5C and sample-0.5P in O_2-saturated 0.1 M KOH solutions with a rotation speed of 1600 rpm and a sweep rate of 10 mV/s.

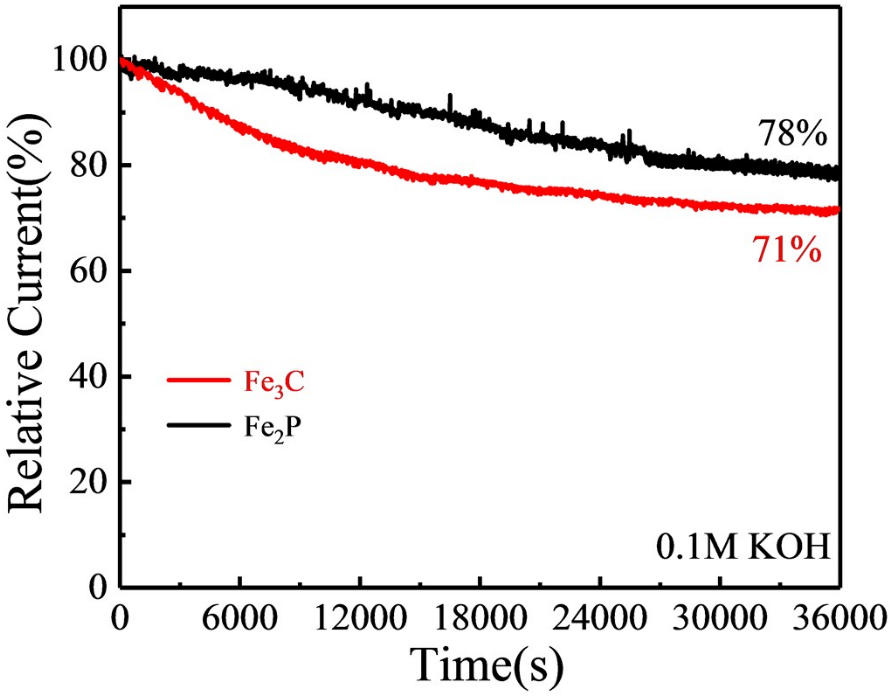

Figure S13. *I–t* curves obtained for ORR with Fe_3C and Fe_2P in 0.1 M KOH solutions.

Table S1. Summary of the potentials for all the compared electrocatalysts at 10 mA/cm^2 (E_{10}) and 100 mA/cm^2 (E_{100}).

	E_{10} (V vs. RHE)	E_{100} (V vs. RHE)
$Fe_2P@Fe_3C$/CNTs	83 mV	364 mV
sample-600	497 mV	702 mV
sample-800	181 mV	312 mV
sample-0.5C	580 mV	685 mV
sample-1.5C	303 mV	433 mV
sample-0.5P	305 mV	425 mV
sample-1.5P	329 mV	462 mV
Fe_3C	383 mV	622 mV
Fe_2P	400 mV	593 mV
25% Pt/C	28 mV	183 mV
Pure GCE	1530 mV	1787 mV

Table S2. The details for calculated fractions of each iron species in the Fe 2p XPS spectrum.

Fraction of each iron species	Fe-C [%]	Fe-P [%]	Fe^{2+} [%]	Fe^{3+} [%]	Satellite
$Fe_2P@Fe_3C$/CNTs	5.55	4.39	61.87	13.59	14.60
$Fe_2P@Fe_3C$/CNTs-200h	4.44	5.53	32.78	52.54	4.71

Table S3. Comparison of HER performance of this work with recently reported similar catalysts in 1.0 M KOH.

Catalysts	E_{10} (V vs. RHE)	Tafel slope (mV/dec)	stability	Reference
Fe_2P@Fe_3C/CNTs	83	53	200 h	This work
Ni-GF/Fe_3C	93	63	20 h	Adv. Energy Mater. 2020, 10, 2002260
FNP	235	76	16 h	Chemical Engineering Journal 390 (2020) 124515
Ni_2P-Fe_2P/NF	128	86	24 h	Adv. Funct. Mater. 2020, 2006484
Fe_3C-Co/NC	238	108.8		Adv. Funct. Mater. 2019, 29, 1901949
Fe_3C@G	264		14 h	Applied Catalysis B: Environmental 248 (2019) 277-285
NHPBAP	121	67	20 h	Adv. Energy Mater. 2018, 1800484
Fe_5C_2-Fe_3C@NC	209	155	1000 cycles	Dalton Trans., 2019,48, 4636-4642
Fe_3C/Mo_2C-1:2	172	87.8	50 h	ChemSusChem 2020,13,5280-5287
P9.03%-(Ni, Fe)$_3S_2$/NF	98	88	15 h	ACS Appl. Mater. Interfaces 2019, 11, 27667-27676
Fe_2P/CoP/Ni_5P_4/RGO	57	47	24 h	ACS Sustainable Chem. Eng. 2019, 7, 13523-13531
0.75-NC-Fe_xP	193	60		ChemElectroChem 2019, 6, 3437-3444
CoFeSP/CNT	130	70	50 h	Electrochimica Acta 318 (2019) 892-900
Ni_2P/Fe_2P/NF	115	193.6	20 h	Journal of Colloid and Interface Science 541 (2019) 279-286
FeCNFs-NP	~250	100		Journal of Power Sources 413 (2019) 367-375
CoFeP NFs/NPCNT	137	64.1	40 h	Nanoscale, 2019, 11, 17031-17040
Ni(OH)$_2$-Fe_2P/TM	76	105	20 h	Chem. Commun., 2018, 54 , 1201-1204

Table S4. Comparison of ORR performance of this work with recently reported similar catalysts in 0.1 M KOH.

Catalysts	E_{onset} (V vs. RHE)	$E_{1/2}$ (V vs. RHE)	n[a)]	Reference
$Fe_2P@Fe_3C/CNTs$	1.06	0.93	3.95	This work
$Fe/Fe_3C@NC$-G-2	0.97	0.88	3.98	Chemical Engineering Journal 401 (2020) 126001
$Fe_3C@MHNFs$		0.9	about 4	J. Mater. Chem. A, 2020,8, 18125-18131
Fe_2N/C	1	0.86	3.97	Nano Research 14, 122-130 (2021)
CNCo-5@Fe-2	0.971	0.861	3.9	Applied Catalysis B: Environmental 261 (2020) 118224
C-ZIF/LFP	0.98	0.88	3.92	Nano Research 13, 818–823 (2020)
CNS-900	0.976	0.844	3.96	J. Mater. Chem. A, 2019, 7, 11321-11330
Fe_2P/NPC	0.997	0.872	3.95~3.99	Carbon 158 (2020) 885-892
Fe_3C-Co/NC	0.94	0.885	3.9	Adv. Funct. Mater. 2019, 29, 1901949
$Fe_3C/NCNF$	1.012	0.873	~3.98	Carbon 142 (2019) 115-122
Fe-NSDC	0.96	0.84	above 3.8	Small 2019, 1900307
$Fe_3C/Fe_2O_3@NGNs$		0.86	3.94	Carbon 146 (2019) 763-771
$Fe_3C@Fe$,N,S-GCM	0.98	0.779	3.92	Carbon 150 (2019) 93-100
$Fe_3C@NP$-PCFs	0.9037	0.8015	~3.98	J. Mater. Chem. A, 2019, 7, 17923-17936
$Fe_3C@NSC/900$	1.059	0.938	3.94~3.97	J. Mater. Chem. A, 2019, 7, 16920-16936
Fe-SAs/Fe_3C-Fe@NC		0.93	3.9	Small 2019, 1906057
$FeS/Fe_3C@NS$-C-900	1.03	0.78	3.93	ACS Appl. Mater. Interfaces 2020, 12, 44710-44719
Fe/N/C-1000-0.05	0.98	0.86		ACS Sustainable Chem. Eng. 2020, 8, 3208-3217
CoFe/FeNC		0.832	3.98	ACS Sustainable Chem. Eng. 2020, 8, 9009-9016
Fe−NCNWs		0.91	3.98	ACS Catal. 2019, 9, 5929-5934
D-BNGFe-2-900	0.95	0.82	3.96	ACS Sustainable Chem. Eng. 2019, 7, 19104-19112

FeCN-S-800	0.91	0.76	3.99	ACS Sustainable Chem. Eng. 2019, 7, 3185-3194
Fe/Fe_3C@NC/CB	0.93	0.83	3.91~4.00	Journal of Materials Science & Technology 35 (2019) 2543-2551
C-FeTA@g-C_3N_4-950-0.5	0.99	0.86	3.9	Journal of Power Sources 417 (2019) 117-124
Fe-N_x-C-1	0.93	0.85		Journal of Power Sources 412 (2019) 125-133
Fe-N/P-C-700	0.941	0.867	3.94	J. Am. Chem. Soc. 2020, 142, 2404-2412
Fe_2P(3 nm)@BC	0.96	0.82	3.9	Journal of Power Sources 435 (2019) 226770

[a] the electron transfer numbers (n).

Table. S5. Summary of Onset potential (E_{oneset}) and half-wave potential ($E_{1/2}$) for all the compared electrocatalysts in O_2-saturated 0.1 M KOH solutions with a rotation speed of 1600 rpm and a sweep rate of 10 mV/s.

	E_{onset} (V vs. RHE)	$E_{1/2}$ (V vs. RHE)	I_d (mA/cm^2)
$Fe_2P@Fe_3C$/CNTs	1.060 V	0.930 V	4.4 mA/cm^2
sample-600	0.855 V	0.685 V	0.55 mA/cm^2
sample-800	1.025 V	0.865 V	3 mA/cm^2
sample-0.5C	0.775 V	0.645 V	0.7 mA/cm^2
sample-1.5C	1.020 V	0.910 V	4.5 mA/cm^2
sample-0.5P	1.055 V	0.875 V	2.5 mA/cm^2
sample-1.5P	0.805 V	0.805 V	1.0 mA/cm^2
Fe_3C	0.970 V	0.840 V	4 mA/cm^2
Fe_2P	0.830 V	0.665 V	0.65 mA/cm^2
25% Pt/C	1.040 V	0.870 V	2.75 mA/cm^2